technical transactions

No. 2020/040

mechanics

sciendo

Analysis of the 2D motion of a monolith platform mechanism

Mikołaj Czyrnek

mikolaj.czyrnek@gmail.com | https://orcid.org/0000-0002-2433-4836

Student of the Doctoral School at Cracow University of Technology

Grzegorz Tora

grzegorz.tora@pk.edu.pl | https://orcid.org/0000-0002-2306-319X

Laboratory of Techno-Climatic Research and Heavy Duty Machines, Faculty of Mechanical Engineering, Cracow University of Technology

Scientific Editor: Stanisław Młynarski, Cracow University of Technology
Technical Editors: Aleksandra Urzędowska, Małgorzata Sikora, Cracow University of Technology Press
Language Editor: Tim Churcher, Big Picture
Typesetting: Anna Basista, Cracow University of Technology Press

Received: September 19, 2020
Accepted: December 11, 2020

Copyright: Copyright: © 2020 Czyrnek, Tora. This is an open access article distributed under the terms of the Creative Commons Attribution License, which permits unrestricted use, distribution, and reproduction in any medium, provided the original author and source are credited.

Data Availability Statement: All relevant data are within the paper and its Supporting Information files.

Competing interests: The authors have declared that no competing interests exist.

Czyrnek, M., Tora, G. (2020). Analysis of the 2D motion of a monolith platform mechanism. *Technical Transactions*, e2020040. https://doi.org/10.37705/TechTrans/e2020040

Abstract

This paper summarises the results of motion analysis of a platform mechanism with a monolith design. A four-link planar mechanism was engineered in which the platform positioning is effected via one passive link and two eccentric links actuated by stepper motors. The prototype of the device was fabricated following a computation procedure based on the classical mechanism and machine theory and FEM calculations. Testing performed on the model and on the real device revealed the presence of two points on the platform for which the resultant of two independent perpendicular displacements implemented by two stages can be obtained for small values of angular displacement.

Keywords: platform mechanisms, monolith designs

1. Platform mechanisms and monolith designs

In recent years, there has been a rapid growth of developments of novel monolithic mechanisms due to their wide range of potential applications in micro-manipulation. Typical monolithic structures are 2D designs cut out from a metal strip and comprising one element with an intricate contour. A decided advantage of monolithic mechanisms is that flexure hinges (Lijian Li et al.; Xiaofeng Li, Yangmin Li) acting as revolute joints are clearance free when in motion. The translational motion effect can be achieved through the use of a monolithic design based on a parallel mechanism; alternatively, the Roberts linkage can be used, yielding a more complicated structure (Sicong Wan, Qingsong Xu). The simplest solution to effect the translational motion is through the use of an acceptably small circular arc configuration (Ke-qi Qi et al.). Flexure-based motions in lieu of joint revolutions should be performed in the elastic range, which improves the fatigue endurance of the hinge material and ensures the geometric repeatability of acting deformations. In practical terms, the maximal elastic flexure acting on the hinge is of the order of one degree (Gawlik A. et al.]. The rotation range can be extended through the use of serial combinations of multiple flexure segments (Guangbo Haoa et al.).

Platform mechanisms incorporate a multi-segment platform with interconnected links or stages effecting the position control. The parallel structure of platform mechanisms results in high stiffness, a relatively small motion range and smaller values of positioning errors. These features render such mechanisms most adequate for use in micro-manipulators executing micro-displacements, both planar (Rui Lina and others; Xiaofeng Li, Yangmin Li) and spatial (Haiyang Li, Guangbo Hao; Junnan Qian and others; Xiaozhi Zhang, Qingsong Xu; Yangmin Lia, Zhigang Wua). However, whilst small stage displacements produce the desired straight-line motion with sufficient precision, the range of angular motion is found to be too small to ensure the required manipulation capability (Ruizhou Wang, Xianmin Zhang; Zeyi Wu, Qingsong Xu).

These features render monolithic structures and platform mechanisms most adequate for applications in micro-positioning systems. In some embodiments monolithic structures incorporate a piezoelectric actuator; thus, their motion range is small, creating the need for a multiplying gear mechanism. Consequently, the error due to the hysteresis becomes more significant (Jiangkun Shang et al.). The application of feedback control offers a solution to this problem. Stepper motors executing a range of revolute motion of 60° require the use of a reduction stage in order for the error involved in angular positioning of the drive shaft to be minimised.

Typically, the first stage in the study of monolith mechanisms involves their conceptual design, underpinned by the classical theory of machines and mechanisms theory such that the adopted parameters can be readily verified. More accurate results as well as stress and strain data are obtained from the FEM analysis (Rouhani E., Nategh). Thus, obtained FEM data are further utilised to engineer a real device complete with a dedicated control system, ultimately the properties of the mechanism are duly verified.

2. Composition of displacements at selected points of the platform

The main aim of the platform in the investigated manipulator is to add independent displacements induced by the two actuators (Zaitsev et al.; Gawlik A. et. al.). Platform 4 represented by a square $CDHQ$ with side a (Fig. 1) is actuated by stage 1 via connector 5 and by stage 2, via connector 6. Connector 5 is found along line CQ and connector 6 is located along extension line HQ. Furthermore, hinge D of platform 4 is able to move at an angle of 45° with respect to the direction of acting stage l and 2 action. In this position, the total displacement of point Q is the resultant of small displacements dx and dy.

https://doi.org/10.37705/TechTrans/e2020040

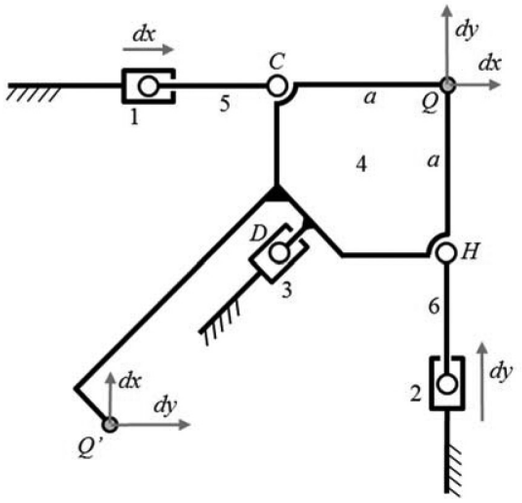

Fig. 1. Points of displacement composition on a 2D platform

The other point on platform 4 where the resultant displacements are readily obtained is point Q', which is found along the direction coinciding with the diagonal DQ, at distance $Q'D$ which is equal to QD. The displacement dx at Q' is executed in the direction dy.

This study outlines the theoretical backgrounds highlighting the properties of points Q and Q' and summarises the results of computer modelling and real-object measurements.

3. Kinematics of platform mechanisms

The real mechanism of the manipulator has to include only revolute joints. Small displacements of links 1 and 2 from Fig. 1 are replaced by small displacements of points B and G along the arcs of circles; thus, the basic structural design will be that shown in Fig. 2. A planar mechanism comprises six stages and includes revolute joints: A, B, C, D, E, F, G, H. The mechanism is actuated by stages 1 and 2, the movements of which are transmitted onto platform 4 via connectors 5 and 6. Platform 4 is connected to the base via connector 3.

Angular positions of double-connector links 1, 2, 3, 5, 6 are defined by versors $\hat{\boldsymbol{i}}_{AB}$, $\hat{\boldsymbol{i}}_{FG}$, $\hat{\boldsymbol{i}}_{ED}$, $\hat{\boldsymbol{i}}_{BC}$, $\hat{\boldsymbol{i}}_{GH}$, with the corresponding lengths: l_{AB}, l_{FG}, l_{ED}, l_{BC}, l_{GH}. Versors $\hat{\boldsymbol{i}}_{CD}$, $\hat{\boldsymbol{i}}_{HD}$, $\hat{\boldsymbol{i}}_{DQ}$, $\hat{\boldsymbol{i}}_{DQ'}$ with the corresponding lengths: $l_{CD}, l_{HD}, l_{DQ}, l_{DQ'}$ are associated with platform 4.

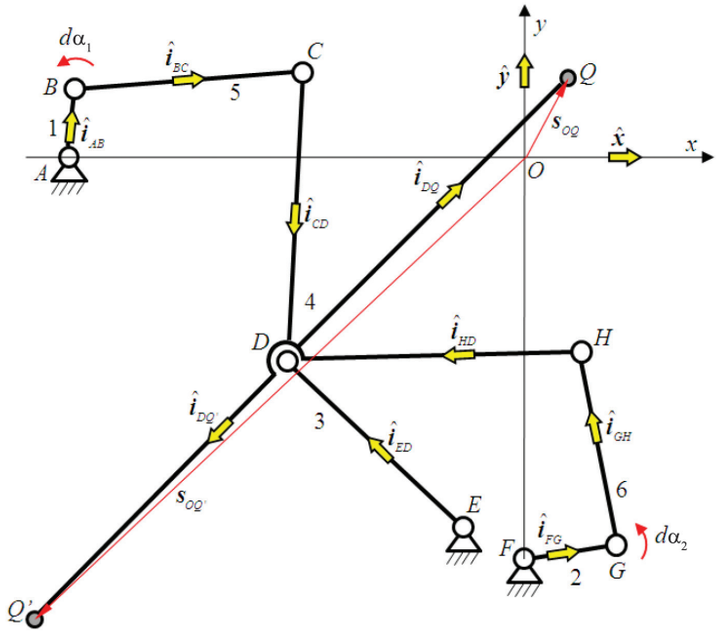

Fig. 2. Structural design of the platform mechanism and relevant versors

The x-axis in the fixed reference systems passes through the centre of hinge A whilst the y-axis passes through the centre of F. The mechanism configuration as well as the position of point Q are defined by three vector equations:

$$\boldsymbol{l}_{AE} + l_{ED}\hat{\boldsymbol{i}}_{ED} = l_{AB}\hat{\boldsymbol{i}}_{AB} + l_{BC}\hat{\boldsymbol{i}}_{BC} + l_{CD}\hat{\boldsymbol{i}}_{CD} \tag{1}$$

$$\boldsymbol{l}_{FE} + l_{ED}\hat{\boldsymbol{i}}_{ED} = l_{FG}\hat{\boldsymbol{i}}_{FG} + l_{GH}\hat{\boldsymbol{i}}_{GH} + l_{HD}\hat{\boldsymbol{i}}_{HD} \tag{2}$$

$$\boldsymbol{s}_{OQ} = \boldsymbol{l}_{OE} + l_{ED}\hat{\boldsymbol{i}}_{ED} + l_{DQ}\hat{\boldsymbol{i}}_{DQ} \tag{3}$$

where:

l_{AE}, l_{FE}, l_{OE} – vectors between fixed points,
$\boldsymbol{s}_{OQ}$ – a variable radius vector of point Q.

Eq. (1), (2) and (3) yield the versor coordinates of mobile passive links, as well as vectors $\boldsymbol{s}_{OQ}$. Upon differentiation, Eq (1) and (2) are projected onto the respective directions $\hat{\boldsymbol{i}}_{BC}$ and $\hat{\boldsymbol{i}}_{GH}$, whilst differentiated equation (3) is projected onto two directions: $\hat{\boldsymbol{x}}$ and $\hat{\boldsymbol{y}}$:

$$l_{ED}d\alpha_3(\hat{\boldsymbol{i}}_{ED}\times\hat{\boldsymbol{i}}_{BC})\hat{\boldsymbol{z}} = l_{AB}d\alpha_1(\hat{\boldsymbol{i}}_{AB}\times\hat{\boldsymbol{i}}_{BC})\hat{\boldsymbol{z}} + l_{CD}d\alpha_4(\hat{\boldsymbol{i}}_{CD}\times\hat{\boldsymbol{i}}_{BC})\hat{\boldsymbol{z}} \tag{4}$$

$$l_{ED}d\alpha_3(\hat{\boldsymbol{i}}_{ED}\times\hat{\boldsymbol{i}}_{GH})\hat{\boldsymbol{z}} = l_{FG}d\alpha_2(\hat{\boldsymbol{i}}_{FG}\times\hat{\boldsymbol{i}}_{GH})\hat{\boldsymbol{z}} + l_{HD}d\alpha_4(\hat{\boldsymbol{i}}_{HD}\times\hat{\boldsymbol{i}}_{GH})\hat{\boldsymbol{z}} \tag{5}$$

$$dx_Q = -l_{ED}d\alpha_3(\hat{\boldsymbol{i}}_{ED}\hat{\boldsymbol{y}}) - l_{DQ}d\alpha_4(\hat{\boldsymbol{i}}_{DQ}\hat{\boldsymbol{y}}) \tag{6}$$

$$dy_Q = l_{ED}d\alpha_3(\hat{\boldsymbol{i}}_{ED}\hat{\boldsymbol{x}}) + l_{DQ}d\alpha_4(\hat{\boldsymbol{i}}_{DQ}\hat{\boldsymbol{x}}) \tag{7}$$

From (4), (5) yields:

$$\begin{bmatrix} l_{ED}(\hat{\boldsymbol{i}}_{ED}\times\hat{\boldsymbol{i}}_{BC})\hat{\boldsymbol{z}} & -l_{CD}(\hat{\boldsymbol{i}}_{CD}\times\hat{\boldsymbol{i}}_{BC})\hat{\boldsymbol{z}} \\ l_{ED}(\hat{\boldsymbol{i}}_{ED}\times\hat{\boldsymbol{i}}_{GH})\hat{\boldsymbol{z}} & -l_{HD}(\hat{\boldsymbol{i}}_{HD}\times\hat{\boldsymbol{i}}_{GH})\hat{\boldsymbol{z}} \end{bmatrix}\begin{bmatrix} d\alpha_3 \\ d\alpha_4 \end{bmatrix} = \begin{bmatrix} l_{AB}(\hat{\boldsymbol{i}}_{AB}\times\hat{\boldsymbol{i}}_{BC})\hat{\boldsymbol{z}} & 0 \\ 0 & l_{FG}(\hat{\boldsymbol{i}}_{FG}\times\hat{\boldsymbol{i}}_{GH})\hat{\boldsymbol{z}} \end{bmatrix}\begin{bmatrix} d\alpha_1 \\ d\alpha_2 \end{bmatrix} \tag{8}$$

and from (6), (7) yields:

$$\begin{bmatrix} dx_Q \\ dy_Q \end{bmatrix} = \begin{bmatrix} -l_{ED}(\hat{\boldsymbol{i}}_{ED}\hat{\boldsymbol{y}}) & -l_{DQ}(\hat{\boldsymbol{i}}_{DQ}\hat{\boldsymbol{y}}) \\ l_{ED}(\hat{\boldsymbol{i}}_{ED}\hat{\boldsymbol{x}}) & l_{DQ}(\hat{\boldsymbol{i}}_{DQ}\hat{\boldsymbol{x}}) \end{bmatrix}\begin{bmatrix} d\alpha_3 \\ d\alpha_4 \end{bmatrix} \tag{9}$$

Thus, the derived system of matrix equations (8) and (9) can be recast as a one matrix equation:

$$\mathrm{d}\mathbf{Q} = \mathbf{J}_Q\mathrm{d}\boldsymbol{\alpha} \tag{10}$$

where:

$\mathrm{d}\mathbf{Q} = \begin{bmatrix} dx_Q \\ dy_Q \end{bmatrix}$ – matrix of orthogonal displacements of point Q,

$\mathrm{d}\boldsymbol{\alpha} = \begin{bmatrix} d\alpha_1 \\ d\alpha_2 \end{bmatrix}$ – matrix of angular displacements of the stages,

$$\mathbf{J}_Q = \begin{bmatrix} -l_{ED}(\hat{\boldsymbol{i}}_{ED}\hat{\boldsymbol{y}}) & -l_{DQ}(\hat{\boldsymbol{i}}_{DQ}\hat{\boldsymbol{y}}) \\ l_{ED}(\hat{\boldsymbol{i}}_{ED}\hat{\boldsymbol{x}}) & l_{DQ}(\hat{\boldsymbol{i}}_{DQ}\hat{\boldsymbol{x}}) \end{bmatrix}\begin{bmatrix} l_{ED}(\hat{\boldsymbol{i}}_{ED}\times\hat{\boldsymbol{i}}_{BC})\hat{\boldsymbol{z}} & -l_{CD}(\hat{\boldsymbol{i}}_{CD}\times\hat{\boldsymbol{i}}_{BC})\hat{\boldsymbol{z}} \\ l_{ED}(\hat{\boldsymbol{i}}_{ED}\times\hat{\boldsymbol{i}}_{GH})\hat{\boldsymbol{z}} & -l_{HD}(\hat{\boldsymbol{i}}_{HD}\times\hat{\boldsymbol{i}}_{GH})\hat{\boldsymbol{z}} \end{bmatrix}^{-1}\begin{bmatrix} l_{AB}(\hat{\boldsymbol{i}}_{AB}\times\hat{\boldsymbol{i}}_{BC})\hat{\boldsymbol{z}} & 0 \\ 0 & l_{FG}(\hat{\boldsymbol{i}}_{FG}\times\hat{\boldsymbol{i}}_{GH})\hat{\boldsymbol{z}} \end{bmatrix}$$

– expressed as displacement components on the plane containing point Q, $\hat{\boldsymbol{z}} = \hat{\boldsymbol{x}}\times\hat{\boldsymbol{y}}$.

The system of equations (1), (2), (3) and (4) constitutes a kinematic model of a platform mechanism based on the classical mechanism and machine theory. Apart from stage 3, the desired geometry of the mechanism will be that of a symmetrical configuration with respect to the straight line passing through point O in the reference frame and inclined at 45° to the horizontal axis, thus the lengths of respective links become: $l_{CD} = l_{HD} = l_p$, $l_{AB} = l_{FG} = l$, $l_{DQ} = l_p\sqrt{2}$. For the initial position of the mechanism, vector coordinates of respective links become: $\hat{\boldsymbol{i}}_{ED}\left(-\sqrt{2}/2,\sqrt{2}/2\right)$, $\hat{\boldsymbol{i}}_{DQ}\left(\sqrt{2}/2,\sqrt{2}/2\right)$, $\hat{\boldsymbol{i}}_{BC}(1,0)$, $\hat{\boldsymbol{i}}_{CD}(0,-1)$, $\hat{\boldsymbol{i}}_{GH}(0,1)$, $\hat{\boldsymbol{i}}_{HD}(-1,0)$, $\hat{\boldsymbol{i}}_{AB}(0,1)$, $\hat{\boldsymbol{i}}_{FG}(1,0)$.

Consequently, we get $\mathbf{J}_Q = l\begin{bmatrix} -1 & 0 \\ 0 & 1 \end{bmatrix}$, which indicates that in the initial position, horizontal displacement of point Q is determined by angle α_1, the vertical displacement – by angle α_2. The other point on the platform that displays similar properties is point Q', satisfying the condition: $l_{DQ} = l_{DQ'}$, $\hat{\boldsymbol{i}}_{DQ'}\left(-\sqrt{2}/2,-\sqrt{2}/2\right)$.

https://doi.org/10.37705/TechTrans/e2020040

Consequently, we get $\mathbf{J}_{Q'} = l\begin{bmatrix} 0 & 1 \\ -1 & 0 \end{bmatrix}$, which indicates that in the initial position of the mechanism, the horizontal displacement of point Q' is determined by angle α_2, the vertical displacement – by angle α_1. Negative displacements dx_Q and $dy_{Q'}$ associated with the angular are duly accounted for and revealed by negative signs of the first column elements in matrices $\mathbf{J}_Q$ and $\mathbf{J}_{Q'}$.

When operational, the mechanism assumes the position in the proximity of its initial position; thus, the values of matrix elements in $\mathbf{J}_Q$ and $\mathbf{J}_{Q'}$ will be slightly different from 1, –1 and 0. Matrix elements in and close to or equal to 1 or –1 indicate the conversion of the motion stage into the motion of points Q or Q' in one of the considered directions. Matrix elements close to or equal to 0 indicate the coupling of the stage motion and the motions of Q or Q' in the respective directions.

4. FEM modelling

FEM model tests are aimed at determining the stress loads acting on flexure hinges. When operated properly, the elastic limit of the material from which the monolith mechanism is fabricated should not be exceeded. Too high stress loads necessitate modifications to the design of the structure or the stage working space in order to reduce stress levels. The application of dedicated software allows displacements of points Q and Q' of the monolith to be obtained and benchmarked against the measurement data. The shape of the monolith being modelled is shown in Fig. 3. Its entire surface has been sub-divided into finite elements of the *shell 181* type using the AutoCAD software program. Depending on their specific functions, the elements were assigned different properties. Two values were adopted: 0.3 for fixtures and flexure hinges and 1.6 for the remaining surfaces. All elements of the monolith are assumed to be 6 mm thick. The model is fixed at four points, in the corners of frame 0 and on joint E connecting element 3 with monolith base 0. Simulations of motion are implemented through the application of kinematic excitations to the fixtures. The displacement map shown in Fig. 3 has relevance to the case when the fixture centre remains immobile and the displacement plot displays an arc-shaped pattern due to the eccentric position of fixture centre 5.

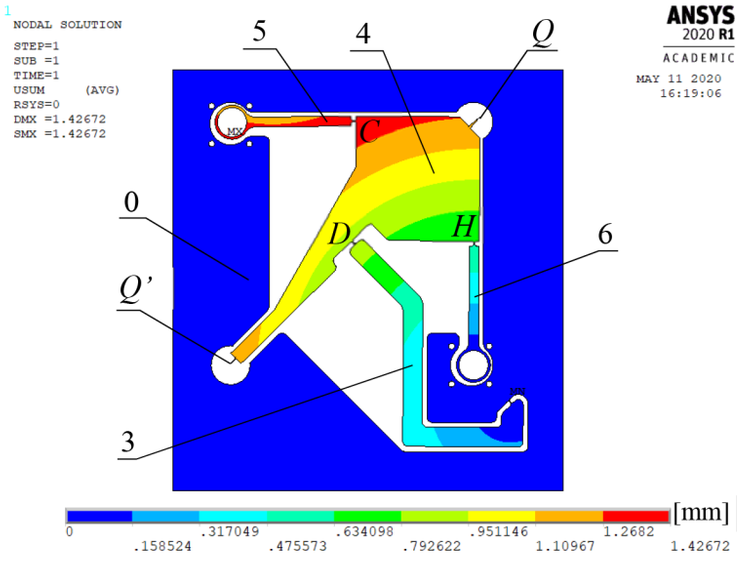

Fig. 3. Distribution of displacements of points

5. Prototype device and investigation of the platform mechanism

The platform mechanism in the monolith configuration shown in Fig. 4 is comprised of a monolith element, two electric drives, a microscope and a control system. The monolith is made from a 6-mm-thick metal strip EN 1.4301. Parts requiring lower manufacturing precision are laser-cut. The flexure hinges and fixtures securing elements 5 and 6 with the mounted bearings are made by spark erosion cutting. The flexure hinges are 0.3 mm thick. The actuators used in this implementation are two JK42HM48-1684 stepper motors mounted to base 0, alongside the TMC 2208 controllers. The motor shafts are eccentrically mounted (2.5 mm off centre) to internal races in rolling bearings attached to fixtures securing elements 5 and 6.

Displacements are registered with a microscope at a magnification of 1:200; the stepper motor control is implemented with Arduino Uno Rev 3 microcontrollers. A dedicated application for controlling the end effector position within the working space is supported by the C# language with the AccelSteppers library.

The control is implemented either manually or with the use of joysticks. In the latter option, the control knob deviations are registered and uniform motions are executed accordingly.

The dedicated numerical simulation program stores the respective monolith positions and, based on coordinates thus registered, the displacement and velocity is computed and the motion of the mechanism implemented.

Fig. 4. Monolithic mechanism measuring station

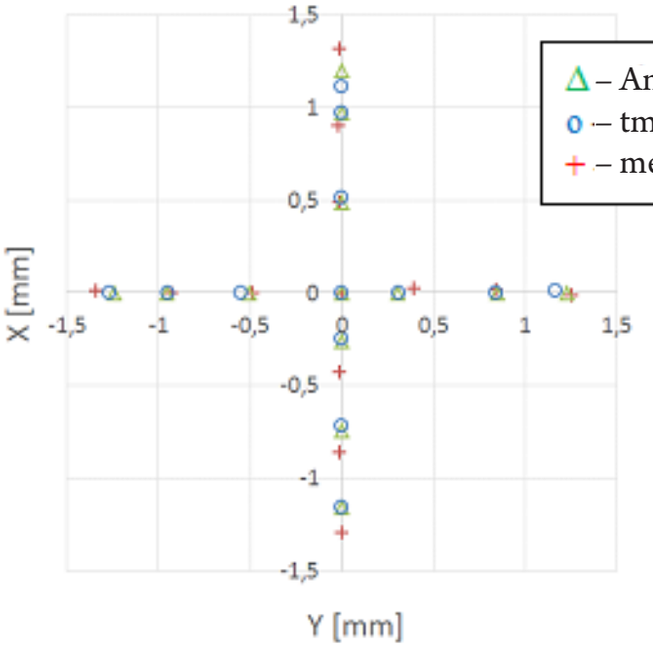

Fig. 5. Positions of point Q

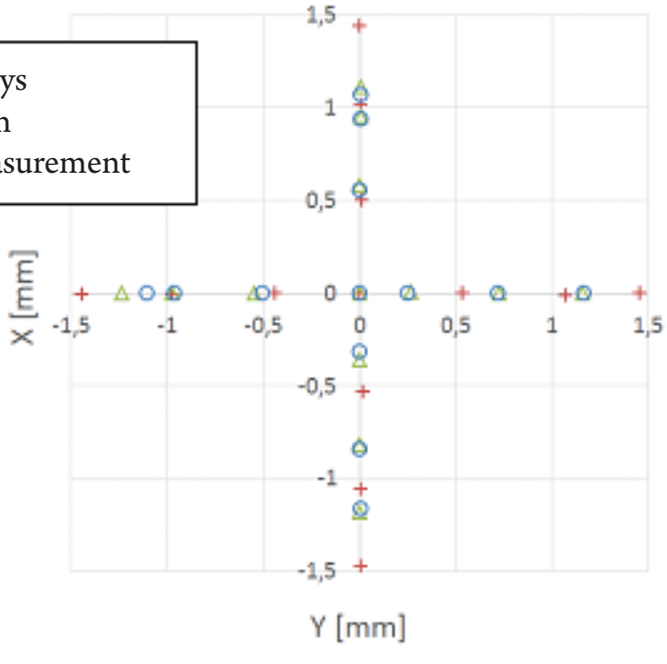

Fig. 6. Positions of point Q'

6. Measurement procedure and results

The measurement procedure started with stage 1 being activated in the range from –30° to 30°, with steps of 10° to execute the displacement of point Q in the Ox direction, whilst stage 2, implementing the displacement of Q in the Oy direction, remained immobilised in the position α_2 = 0°. Following each

https://doi.org/10.37705/TechTrans/e2020040

step variation of α_1, the coordinates of point Q were registered with the use of a microscope. Next, the roles of the two stages were switched. With the microscope being moved to the new position, an identical procedure was adopted to measure the displacements of point Q'. The plot in Fig. 5 shows the positions of Q derived from theoretical modelling, FEM calculations and measurements. In the theoretical calculations (tmm), the following dimensions were assumed: $L_{AB} = l_{FG} = 2.5$ mm, $L_{ED} = 184.2$ mm, $L_{BC} = l_{GH} = 100.0$ mm, $L_{CD} = l_{HD} = 100.0$ mm, $L_{DQ} = l_{DQ'} = 141.4$ mm. A variation of the point Q position on the Ox axis corresponds to the angular displacement of stage 1, whilst the change of its position on the Oy axis is registered as the angular displacement of stage 2. The plot in Fig. 6 illustrates the positions of point Q'; the change of Q' position on the Ox axis corresponds to the angular displacement of stage 2 whilst the change of its position on the Oy axis gives the angular displacement of stage 1. In Fig. 5, the coordinates of point Q are plotted in the reference frame with its origin shifted by $-s_{OQ}$ for $\alpha_1 = \alpha_2 = 0$, whilst in Fig. 6, the coordinates of point Q' are plotted against the reference frame whose origin is shifted by $-s_{OQ'}$ for $\alpha_1 = \alpha_2 = 0$.

The analysis of the extreme positions of points Q and Q' yields the motion conversion ratio summarised in Table 1.

Table 1. Motion transmission ratio for points Q and Q'

[mm/°]	Measurement	FEM model	Tmm model
k_Q	0.0433	0.0400	0.0417
$k_{Q'}$	0.0483	0.0396	0.0417

7. Conclusions

The theoretical studies, model tests and measurements taken on a real object have demonstrated that when the mechanism remains in its initial position, the total displacement of point Q is found as the resultant of its horizontal displacement induced by stage 1 and the vertical displacement associated with stage 2. In the case of point Q', its displacement is the resultant of its horizontal displacement induced by stage 2 and vertical displacement due to stage 1. Actually, the motion of Q' is the inverse of the motion components for point Q.
The resultant motions of stages 1 and 2 at point Q were easy to predict whilst similar properties of point Q' were established recalling the theoretical model of the manipulator mechanism, yielding the motion transmission ratio and motion coupling of Q and Q' points that were close to the real values.
Thus, point Q' can be regarded as an alternative for Q, i.e. another point where a tool can be fixed within the structure of a monolith platform mechanism, permitting the resultant displacements to be determined.

References

Gawlik, A., Harmatys, W., Łaczek, S., Tora, G. (2019). Manipulator effecting 2D microdisplacements. *Advances in Mechanism and Machine Science. Mechanisms and Machine Science*, 73, 1829–1838.

Guangbo, Haoa, Xiuyun, He, Shorya, Awtar (2019). Design and analytical model of a compact flexure mechanism for translational motion. *Mechanism and Machine Theory*, 142, 1–24.

Haiyang, Li, Guangbo, Hao (2015). A constraint and position identification (CPI) approach for the synthesis of decoupled spatial translational compliant parallel manipulators. *Mechanism and Machine Theory*, 90, 59–83.

Jiangkun, Shang, Yanling, Tian, Zheng, Li, Fujun, Wang, Kunhai, Cai (2015). A novel voice coil motor-driven compliant micropositioning stage based on flexure mechanism. *Review of Scientific Instruments*, 86, 1–10.

Junnan, Qian, Yangmin, Li, Lukai, Zhuge (2020). An Investigation on a Novel 3-RCU Flexible Micromanipulator. *Micromachines*, 423, 1–11.

Ke-qi, Qi, Ya-lin, Ding, Yang, Xiang, Chao, Fang, Yang, Zhang (2017). A novel 2-DOF compound compliant parallel guiding mechanism. *Mechanism and Machine Theory*, 117, 21–34.

Lijian, Li, Dan, Zhang, Sheng, Guo, Haibo, Qu (2019). Design, modeling, and analysis of hybrid flexure hinges. *Mechanism and Machine Theory*, 131, 300–316.

Rouhani, E., Nategh, M.J. (2016). An elastokinematic solution to the inverse kinematics of microhexapod manipulator with flexure joints of varying rotation center. *Mechanism and Machine Theory*, 97, 127–140.

Rui, Lina, Yingzi, Li, Yingxu, Zhang, Tingwei, Wanga, Zhenyu, Wanga, Zihang, Songa, Zhipeng, Doua, Jianqiang, Qiana (2019). Design of A flexure-based mixed-kinematic XY high-precision positioning platform with large range. *Mechanism and Machine Theory*, 142, 1–16.

Ruizhou, Wang, Xianmin, Zhang (2017). Optimal design of a planar parallel 3-DOF nanopositioner with multi-objective. *Mechanism and Machine Theory*, 112, 61–83.

Sicong, Wan, Qingsong, Xu (2016). Design and analysis of a new compliant XY micropositioning stage based on Roberts mechanism. *Mechanism and Machine Theory*, 95, 125–139.

Xiaofeng, Li, Yangmin, Li (2013). Design and Analysis of a 2-DOF Micro-motion Stage based on Differential Amplifier. In: Proceedings of the 13th IEEE International Conference on Nanotechnology (472–477). Beijing.

Xiaozhi, Zhang, Qingsong, Xu (2018). Design, fabrication and testing of a novel symmetrical 3-DOF large-stroke parallel micro/nano-positioning stage. *Robotics and Computer–Integrated Manufacturing*, 54, 162–172.

Yangmin, Lia, Zhigang, Wua (2016). Design, analysis and simulation of a novel 3-DOF translational micromanipulator based on the PRB model. *Mechanism and Machine Theory*, 100, 235–258.

Zaitsev, W.A., Raikhman, Ja.A., Bykovski P.A. (1978). Mikromanipulator, Patent no. 590536.

Zeyi, Wu, Qingsong, Xu (2018). Design, optimization and testing of a compact XY parallel nanopositioning stage with stacked structure. *Mechanism and Machine Theory*, 126, 171–188.

https://doi.org/10.37705/TechTrans/e2020040

Badanie ruchu 2D platformowego mechanizmu monolitycznego

Streszczenie: Artykuł zawiera wyniki badań ruchu mechanizmu platformowego wykonanego w technologii monolitu. Zaprojektowano i wykonano czteroogniwowy mechanizm płaski, w którym platforma jest pozycjonowana przez jedno ogniwo bierne oraz przez dwa ogniwa mimośrodowe poruszane silnikami krokowymi. Po wstępnych obliczeniach klasycznego modelu tmm mechanizmu i następnie obliczeniach MES wykonano prototyp urządzenia. Badania modelowe i rzeczywistego obiektu wykazały, że na platformie znajdują się dwa punkty, w których można składać dla małych przemieszczeń kątowych dwa niezależne, prostopadłe przemieszenia pochodzące od napędów.

Słowa kluczowe: mechanizmy platformowe, mechanizmy monolityczne